An Adaptive Feedback Linearization Approach to Inertial Frequency Response of Wind Turbines

Mohammadreza Toulabi, Ahmad Salehi Dobakhshari, and Ali Mohammad Ranjbar

***Abstract*—Synthetic inertial frequency response has attracted increasing attention due to the paradigm shift in power generation from synchronous generators toward wind turbines. This paper presents a novel nonlinear controller to enable inertial response of a variable speed wind turbine (VSWT). The VSWT has a nonlinear model which cannot efficiently be dealt with by linear control techniques as it may experience large deviations from its operating point during the frequency support period. To design the controller, a nonlinear model for the wind turbine together with power system is utilized. The output power of the wind turbine is expressed in terms of the state variables, and its exact Taylor series expansion is used in control design procedure. A regular controller is first designed based on the input–output feedback linearization approach. Then, the regular controller is replaced by an adaptive one to accommodate parameter variations of VSWT. The proposed controller is then embedded in the detailed model of the VSWT in MATLAB/Simulink environment. Extensive investigations, including the effects of different controller parameters, are carried out. Impacts of the most important practical operational constraints in the VSWT inertia response are also analyzed. Results verify the superiority and appropriateness of the proposed controller.**

***Index Terms*—Auxiliary controller, frequency support, inertial response, recovery period, variable speed wind turbine (VSWT).**

I. Introduction

WIND power has been the fastest growing source of energy in the past two decades, skyrocketing from 6 GW installed capacity in 1996 to 400 GW today. This figure will keep rising as, for example, the 2-degrees scenario for cutting emission requires the world to generate 11 times more wind power by 2050 [1]. In the United States, wind alone is estimated to supply 20% of the electricity by 2030 [2], even though the US has the potential for more than 10000 GW of onshore wind power [3]. In 2014, cumulative wind market growth in the EU was 10.5% as the European wind energy industry installed more new wind capacity than gas and coal combined [4].

These figures urge for active contribution of wind farms in technical aspects of power system operation. In particular, the problem of frequency regulation in systems with high penetration of wind power is twofold: On the one hand, the overall system inertia will be decreased as wind turbine generators get decoupled from the grid by power electronics converters, which leads to deterioration in frequency regulation. On the other hand, the kinetic energy stored in turbine blades together with fast power electronic controllers creates an opportunity to swiftly adjust wind power output in response to frequency excursions [5, p. 80].

Although the control of wind energy conversion systems (WECSs) is a challenging task due to nonlinear dynamics in their models [6, p. 3], different methods for implementing the frequency controller into WESCs have been proposed. In so doing, popular solutions include inertial control [7], [8], droop control [9], [10] and both [11], [12]. The inertial control loop causes the wind turbine to emulate the synchronous machine inertial behavior.

To facilitate large-scale integration of wind farms in power systems, several manufacturers such as GE [13] and Enercon [14] have included inertial response feature in their turbines.

Although it has been shown that replacement of synchronous generators by wind turbines can have an adverse impact on system inertia and limit the wind penetration level [15], the inertial response by wind turbines has yielded promising results in the US Eastern [8] and Western [16] interconnections. From a market point of view, frequency response by wind turbines reduces grid operation costs by decreasing the amount of required spinning reserve [17].

In most of previous research works, the output power of a VSWT for power system inertial control is adjusted using a conventional controller such as PI controller. In fact, the strategy of frequency support in the VSWT is to change the torque set point as the power system frequency is perturbed. Other advanced methods based on the linearized model of WECS have been developed, which utilize model predictive control [18] and variable gains for inertial response using shape functions [19]. However, since all of the above methods are based on a linearized model of WECS, their performance degrades significantly when there is a large deviation from the operating point.

To overcome the inadequacies of previous controllers, this paper proposes the application of a novel nonlinear frequency controller based on the feedback linearization technique. The paper comprises of two main sections, i.e., controller design and controller analysis. Since in the inertial frequency response only a small time interval after the disturbance, which involves rate of change of frequency and frequency nadir, are of interest,

Manuscript received March 19, 2016; revised June 29, 2016 and October 17, 2016; accepted November 19, 2016. Date of publication November 22, 2016; date of current version June 17, 2017. Paper no. TSTE-00216-2016.

M. Toulabi and A. M. Ranjbar are with the School of Electrical Engineering, Sharif University of Technology, Tehran 11365-11155, Iran (e-mail: toulabi@ee.sharif.edu; amranjbar@sharif.edu).

A. S. Dobakhshari is with the Department of Electrical Engineering, Faculty of Engineering, University of Guilan, Rasht 41996-13776, Iran (e-mail: salehi_ahmad@guilan.ac.ir).

Color versions of one or more of the figures in this paper are available online at http://ieeexplore.ieee.org.

Digital Object Identifier 10.1109/TSTE.2016.2631579

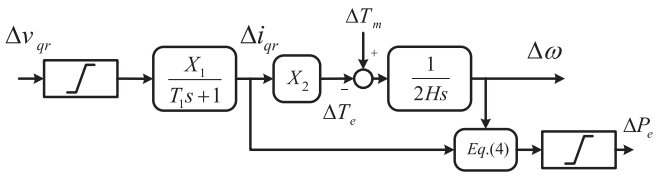

Fig. 1. Wind turbine simple model for frequency studies.

the slow dynamics (such as the turbine/governor) are ignored in the design part. However, in the analysis part, the effects of all involved dynamics are taken into account and all simulations are carried out considering all dynamics. Likewise, it is not necessary to consider the effects of the main controller. This approach is commonly utilized in designing the auxiliary controller for FACTS equipment [20]. The salient features of the proposed approach compared to the conventional controllers are 1) The proposed control is not affected by large deviations from the operating point anticipated during the inertial response and 2) An adaptive scheme has been devised in order to update the controller parameters.

The rest of the paper is organized as follows. In Section II, the nonlinear state space model of the WESC together with the power system is developed. Section III is devoted to the design of the proposed feedback linearization-based controller and evaluating its internal stability. An adaptive scheme is also introduced in order to update the parameters of the controller. Extensive simulations are carried out in Section IV to evaluate the inertial response provided by the proposed controller under different operating conditions, intermittent wind speed and nonlinear constraints on input and output of the WECS. Section V concludes the paper.

II. Model of Power System and Wind Turbine in Frequency Studies

It has been shown that the frequency response of induction generator-based VSWT, i.e., doubly fed induction generators (DFIG) and full power converters (FPC) equipped with induction machines, during the first seconds after system disturbances can be analyzed by a simplified model [21]. This model can be utilized in frequency studies on a single bus equivalent of the power system. With reasonable assumptions, both types show similar transient behaviors and the same model can be considered for VSWTs in the frequency domain analysis [22, p. 299]. This simplified model is depicted in Fig. 1 for the DFIG and described by the following state equations [21]:

$$s\Delta i_{\rm qr} = -\left(\frac{1}{T_1}\right)\Delta i_{\rm qr} + \left(\frac{X_1}{T_1}\right)\Delta v_{\rm qr} \tag{1}$$

$$s\Delta\omega = -\left(\frac{X_2}{2H}\right)\Delta i_{\rm qr} + \left(\frac{1}{2H}\right)\Delta T_m \tag{2}$$

where $i_{\rm qr}$, $v_{\rm qr}$, ω, H, and T_m are rotor quadrature current (pu), rotor quadrature input voltage (pu), rotational speed (pu), inertia constant (s), and input mechanical torque (pu), respectively. All other parameters in these state equations are defined in Table I, where L_m, $L_{\rm rr}$, and $L_{\rm ss}$ are the magnetizing inductance, rotor self-inductance, and stator self-inductance, respectively. Moreover, R_r and R_s are rotor and stator resistances, respectively.

TABLE I
VSWT Simple Model Parameters

WT type	X_1	X_2	T_1
DFIG	$\frac{1}{R_r}$	$\frac{L_m}{L_{\rm ss}}$	$\frac{X_0}{\omega_s R_r}$
FPC	$\frac{1}{R_s}$	$\frac{L_m}{L_{\rm rr}}$	$\frac{X_{\rm ss}}{\omega_s R_s}$
Inductance	$L_0 = L_{\rm rr} - \frac{L_m^2}{L_{\rm ss}}$	$L_{\rm ss} = L_{\rm ls} + L_m$	$L_{\rm rr} = L_{lr} + L_m$

The wind turbine output power based on the above state variables is as follows [22], [23]:

$$P_e = -X_2\omega i_{\rm qr} \tag{3}$$

It should be noted that to formulate this simple frequency model for the FPC type, in (1) to (3), the variables $v_{\rm qr}$ and $i_{\rm qr}$ must be replaced by $v_{\rm qs}$ and $i_{\rm qs}$, respectively. The associated coefficients for the FPC type are given in Table I.

As WECS operates at Maximum Power Point (MPP) normally, its Taylor series expansion is calculated around MPP as follows:

$$\Delta P_e = -X_2\omega_{\rm MPP}\Delta i_{\rm qr} - X_2 i_{\rm qr_{MPP}}\Delta\omega - X_2\Delta i_{\rm qr}\Delta\omega \tag{4}$$

where $i_{\rm qr_{MPP}}$ and $\omega_{\rm MPP}$ are the rotor injected current and speed at MPP, respectively. It should be noted that, in contrast to linearized models used in the literature, there is no approximation in (4).

To complete the state equations needed in the controller design, basic power system frequency model is also needed. In fact, the system frequency is determined by the rotation speed of synchronous generators. The swing equation may be used to express deviation of frequency from its nominal value [24, Ch. 9]:

$$\Delta P_{\rm mech} - \Delta P_{\rm elec} = M\frac{d\Delta f}{dt} \tag{5}$$

where $\Delta P_{\rm mech}$ and $\Delta P_{\rm elec}$ denote changes in mechanical power and electrical power, respectively, and M represents power system acceleration time constant. Moreover, Δf is the change in system frequency. $\Delta P_{\rm mech}$ is a result of governor action of synchronous generators, expressed in Laplace domain as [24, Ch. 9]:

$$\Delta P_{\rm mech}(s) = -\frac{1}{R}T_{\rm Gov}(s)T_{\rm Tur}(s)\Delta f(s) \tag{6}$$

where R characterizes equivalent speed-droop of synchronous generators and $T_{\rm Gov}(s)$ and $T_{\rm Tur}(s)$ reflect dynamics of respectively governors and turbines of conventional synchronous generators. These dynamics have been neglected in the design process as their time constants are much larger than those of the proposed controller, which will be evident from simulations where turbine and governor models will be considered. The same assumption is common in power system frequency studies [24, Ch. 9]. $\Delta P_{\rm elec}$ is the change in produced electric power of the system, expressed as follows:

$$\Delta P_{\rm elec}(s) = \Delta P_L(s) + D\Delta f(s) - \Delta P_e(s) \tag{7}$$

TABLE II
WIND TURBINE SPECIFICATIONS

Parameter	Value (Unit)
Stator Resistance (R_s)	0.00488 pu
Rotor Resistance (R_r)	0.00549 pu
Stator Inductance ($L_{\rm ls}$)	0.09241 pu
Rotor Inductance ($L_{\rm lr}$)	0.09955 pu
Magnetizing Inductance (L_m)	3.95279 pu
Lumped Inertia Constant (H)	3.5 s

where load change is assumed to comprise of frequency-dependent load change $D\Delta f(s)$ (i.e., motor loads) and non-frequency-sensitive load change $\Delta P_L(s)$ [24, Ch. 9]. Besides, ΔP_e is the increase in wind power output, hence the minus sign. Combining (5)-(7) leads to:

$$s\Delta f(s) = -\frac{D}{M}\Delta f(s) + \frac{1}{M}\Delta P_e(s) - \frac{1}{M}\Delta P_L(s) + \frac{1}{RM}\Delta f(s) \tag{8}$$

It should be noted that M, D and R can be the aggregate equivalents considering synchronous generators [22, p. 52], power electronic interfaced distributed generation and frequency-dependent loads models [11].

The WECS model in (1) and (2) in conjunction with the power system representation in (8) are the equations taken into account in controller design process.

From now on, the state variables $\Delta i_{\rm qr}$, $\Delta\omega$, and Δf will be renamed x_1, x_2, and x_3, respectively. This leads to the following aggregated power system and WECS model:

$$\begin{cases} \dot{x}_1 = -\alpha_1 x_1 + \beta u \\ \dot{x}_2 = -\alpha_2 x_1 + \beta_1 w_1 \\ \dot{x}_3 = -\alpha_3 x_3 + \gamma_1 x_1 + \gamma_2 x_2 + \gamma_3 x_1 x_2 - \beta_2 w_2 \end{cases} \tag{9}$$

where

$$\alpha_1 = \frac{1}{T_1}, \quad \alpha_2 = \frac{X_2}{2H}, \quad \alpha_3 = \frac{D}{M} + \frac{1}{RM}$$
$$\beta = \frac{X_1}{T_1}, \quad \beta_1 = \frac{1}{2H}, \quad \beta_2 = \frac{1}{M}$$
$$\gamma_1 = -\frac{X_2\omega_{\rm MPP}}{M}, \quad \gamma_2 = -\frac{X_2 i_{\rm qr_{MPP}}}{M}, \quad \gamma_3 = -\frac{X_2}{M}$$
$$u = \Delta v_{\rm qr}, \quad w_1 = \Delta T_m, \quad w_2 = \Delta P_L$$

It is worth noting that the model adopted concerns a small interval right after the disturbance, as rate of change of frequency and frequency nadir are of interest. This allows to not consider the MPP controller [21]. Likewise, the dynamics of the governors and turbines of synchronous generators have been neglected as their time constants are much larger than those of the proposed controller, which will be evident from simulations.

A 2 MW induction generator-based wind turbine, whose specifications are given in Table II, is studied in this paper. The power system parameters M and D are assumed to be 8 s and 0.8 pu, respectively.

III. CONTROLLER DESIGN AND ANALYSIS

Feedback linearization approach is commonly used to control nonlinear systems. It has been applied in practical and industrial control problems such as the control of helicopters, high performance aircrafts, industrial robots, and biomedical devices. In the simplest form, feedback linearization is an approach which cancels the nonlinearities such that the closed-loop system is transformed into a linear form.

Feedback linearization consists of two main stages. The first stage is the transformation of the nonlinear system into an equivalent linear one. This is accomplished by a suitable change of variables. It should be noted that after this stage system equations become linear at the expense of a nonlinear controller. The second stage is the application of well-known linear control methods to control the equivalent system. The design process based on input-output feedback linearization approach is decomposed into three following steps [25, pp. 509-521]:

1) Determine dynamical system relative degree,
2) Cancel the nonlinearities and guarantee the convergence with an appropriate input u,
3) Investigate stability of the internal dynamics.

A. Regular Controller

To design the controller based on input-output feedback linearization approach, Δf, as the main goal of frequency regulation process, is considered as the overall system output. This leads to the following nonlinear system representation:

$$\dot{\mathbf{x}} = \underbrace{\begin{pmatrix} -\alpha_1 x_1 \\ -\alpha_2 x_1 \\ -\alpha_3 x_3 + \gamma_1 x_1 + \gamma_2 x_2 + \gamma_3 x_1 x_2 \end{pmatrix}}_{\mathbf{f}(\mathbf{x})} + \underbrace{\begin{pmatrix} \beta \\ 0 \\ 0 \end{pmatrix}}_{\mathbf{g}(\mathbf{x})} u + \begin{pmatrix} 0 \\ \beta_1 w_1 \\ -\beta_2 w_2 \end{pmatrix} \tag{10}$$
$$y = x_3$$

where $\mathbf{x} = (x_1, x_2, x_3)^T$. Simple manipulation (calculating the derivative of the output) reveals that the system has the relative degree two in $\{\mathbf{x} \in R^3 | x_2 \neq -\omega_{\rm MPP}\}$, i.e., $\rho = 2$. To transform the overall system into normal form coordinates, the following transformation (change of variables) is utilized:

$$T = \begin{pmatrix} \xi_1 = y \\ \xi_2 = \dot{y} \\ \eta = x_2 \end{pmatrix} \tag{11}$$

where ξ_1, ξ_2, and η are Δf, $\dot{f}$, and $\Delta\omega$, respectively. It should be noted that the latter coordinate (internal dynamics) should be chosen such that $\frac{\partial \eta}{\partial \mathbf{x}}.\mathbf{g}(\mathbf{x}) = 0$ [25, p. 515]. $\eta(\mathbf{x}) = x_2$ is a simple solution to the foregoing partial differential equation. It can be easily seen that the Jacobian matrix of the transformation is nonsingular. In the new coordinates, the overall dynamical

equations are described by:

$$\begin{cases} \dot{\xi}_1 = \xi_2 \\ \dot{\xi}_2 = a(\xi_1, \xi_2, \eta) + b(\xi_1, \xi_2, \eta)u \\ \dot{\eta} = -\dfrac{\alpha_2 \left(\xi_2 + \alpha_3 \xi_1 - \gamma_2 \eta + \beta_2 w_2\right)}{\gamma_1 + \gamma_3 \eta} + \beta_1 w_1 \end{cases} \tag{12}$$

where

$$\begin{aligned} a(\xi_1, \xi_2, \eta) = & -(\alpha_1\gamma_1 + \alpha_2\gamma_2 + \alpha_3\gamma_1)x_1 - \alpha_3\gamma_2\eta \\ & + \alpha_3^2\xi_1 - (\alpha_1\gamma_3 + \alpha_3\gamma_3)x_1\eta - \alpha_2\gamma_3 x_1^2 \end{aligned} \tag{13}$$

$$b(\xi_1, \xi_2, \eta) = \beta\gamma_1 + \beta\gamma_3\eta \tag{14}$$

To verify the feasibility of application of input-output feedback linearization, the stability of zero dynamics part must be verified. In other words, although the closed loop system can be stabilized using input-output feedback linearization, there is no guarantee for stability of the whole dynamics [25, p. 517]. There may exist unobservable mode(s) which construct the internal dynamics of system and can not be seen from the external input-output relationship. If the internal dynamics are stable, the control design problem will be resolved. Otherwise, the instability of the internal dynamics results in undesirable phenomena.

Generally, it is difficult to directly determine the stability of the internal dynamics due to its coupling with the external closed loop dynamics. The Lyapunov analysis can be utilized for special dynamical systems, though, its applicability is limited by the difficulty of finding the Lyapunov function. For the designed controller, however, the analytical solution of internal dynamics can be obtained and its stability can be determined directly. It should be noted that to analyze the embedded inertial controller response, it is assumed that $\Delta P_L = 0$ and $\Delta T_m = 0$. The reason is that each of them play out as a disturbance, and therefore, their impacts are discussed after the design process, separately.

To characterize the zero dynamics, restrict $\mathbf{x}$ to

$$Z^* = \left\{\mathbf{x} \in R^3 | \xi_1 = \xi_2 = 0\right\}$$

This process yields (assume that $w_1 = w_2 = 0$)

$$\dot{\eta} = \frac{\alpha_2\gamma_2\eta}{\gamma_1 + \gamma_3\eta} \tag{15}$$

Equation (15) can be solved to give an analytical solution for the zero dynamics as follows:

$$e^{-\frac{\eta}{\alpha_2 i_{\mathrm{qr_{MPP}}}}} \times \eta^{-\frac{\omega_{\mathrm{MPP}}}{\alpha_2 i_{\mathrm{qr_{MPP}}}}} = F_0 e^{-t}, \tag{16}$$

where F_0 represents the dependency of zero dynamics part to the initial conditions. Since rotational speed ω is always greater than zero, $\eta > -\omega_{\mathrm{MPP}}$, and therefore the first term in the left hand side of (16) cannot tend to zero as t approaches infinity. Thus, the zero dynamics have an asymptotically stable equilibrium point at $\eta = 0$ and the system is minimum phase. Therefore, it is possible to stabilize the overall system using input-output linearization approach. The state feedback control (k_1 and k_2 are controller parameters)

$$u = \frac{1}{b(\xi_1, \xi_2, \eta)}\left(-a(\xi_1, \xi_2, \eta) - k_1\xi_1 - k_2\xi_2\right) \tag{17}$$

results in

$$\begin{pmatrix} \dot{\xi}_1 \\ \dot{\xi}_2 \end{pmatrix} = \begin{pmatrix} 0 & 1 \\ -k_1 & -k_2 \end{pmatrix} \begin{pmatrix} \xi_1 \\ \xi_2 \end{pmatrix} \tag{18}$$

It should be noted that $a(\xi_1, \xi_2, \eta)$ and $b(\xi_1, \xi_2, \eta)$ in the control law (17) are given in (13) and (14), respectively. The only constraint for stability of (18) is that k_1 and k_2 must have positive values.

B. Adaptive Controller

As can be seen in (9) the system dynamics depend on γ_1 and γ_2 which in turn are dependent on ω_{MPP} and $i_{\mathrm{qr_{MPP}}}$, respectively. On the other hand, these optimal rotational speed and rotor current are themselves dependent on wind speed and power-speed characteristics of the wind turbine. Moreover, the rotor blade angle changes continuously to limit the input wind power and thus prevent possible damage to the WECS installation. It can be concluded that γ_1 and γ_2 change continuously. This important fact must be accommodated in the controller design process by transforming the regular controller to an adaptive one. In other words, an estimation algorithm is needed to eliminate the impacts of these unknown parameters. The dynamics of the estimation algorithm are as follow [26, chap. 5]:

$$\dot{\hat{\Gamma}} = \begin{pmatrix} \dot{\hat{\gamma}}_1 \\ \dot{\hat{\gamma}}_2 \end{pmatrix} = N \times r(x_1, x_2, x_3, \hat{\Gamma}) = N \times \begin{pmatrix} r_1 \\ r_2 \end{pmatrix} \tag{19}$$

where $\hat{\gamma}_1$ and $\hat{\gamma}_2$ are the estimation of γ_1 and γ_2, $N = N^T$ is a positive definite matrix and $r(x_1, x_2, x_3, \hat{\Gamma})$ is a smooth function to be determined. Using the following change of variables:

$$\begin{cases} \xi_1 = x_3 \\ \xi_2 = -\alpha_3 x_3 + \hat{\gamma}_1 x_1 + \hat{\gamma}_2 x_2 + \gamma_3 x_1 x_2 \end{cases} \tag{20}$$

and the same control law as above with estimated values for γ_1 and γ_2, i.e.,

$$u = \frac{1}{b(\xi_1, \xi_2, \eta, \hat{\Gamma})}\left(-a(\xi_1, \xi_2, \eta, \hat{\Gamma}) - k_1\xi_1 - k_2\xi_2\right) \tag{21}$$

where

$$\begin{aligned} a(\xi_1, \xi_2, \eta, \hat{\Gamma}) = & (\alpha_1\hat{\gamma}_1 + \alpha_2\hat{\gamma}_2 + \alpha_3\hat{\gamma}_1)x_1 - \alpha_3\hat{\gamma}_2\eta \\ & + \alpha_3^2\xi_1 - (\alpha_1\gamma_3 + \alpha_3\gamma_3)x_1\eta - \alpha_2\gamma_3 x_1^2 \end{aligned} \tag{22}$$

$$b(\xi_1, \xi_2, \eta, \hat{\Gamma}) = \beta\hat{\gamma}_1 + \beta\gamma_3\eta \tag{23}$$

results in

$$\begin{cases} \dot{\xi}_1 = \xi_2 + \tilde{\gamma}_1 x_1 + \tilde{\gamma}_2 x_2 \\ \dot{\xi}_2 = -\alpha_3\tilde{\gamma}_1 x_1 - \alpha_3\tilde{\gamma}_2 x_2 - k_1\xi_1 - k_2\xi_2 \\ \dot{\hat{\Gamma}} = N \times r(x_1, x_2, x_3, \hat{\Gamma}) \end{cases} \tag{24}$$

where $\tilde{\Gamma} = \begin{pmatrix} \tilde{\gamma}_1 \\ \tilde{\gamma}_2 \end{pmatrix} = \Gamma - \hat{\Gamma}$ is the error vector of the estimation algorithm. Considering

$$V = \frac{1}{2}\xi_1^2 + \frac{1}{2}\xi_2^2 + \frac{1}{2}\tilde{\Gamma}^T N^{-1}\tilde{\Gamma} \tag{25}$$

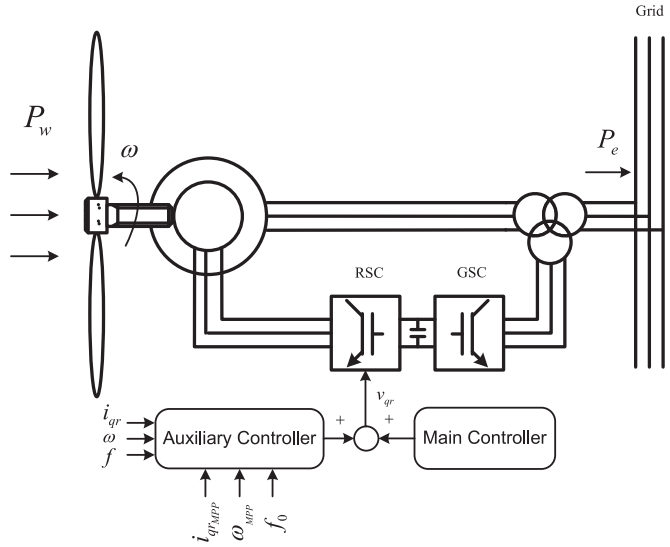

Fig. 2. General structure of DFIG-based wind turbine equipped with the proposed controller.

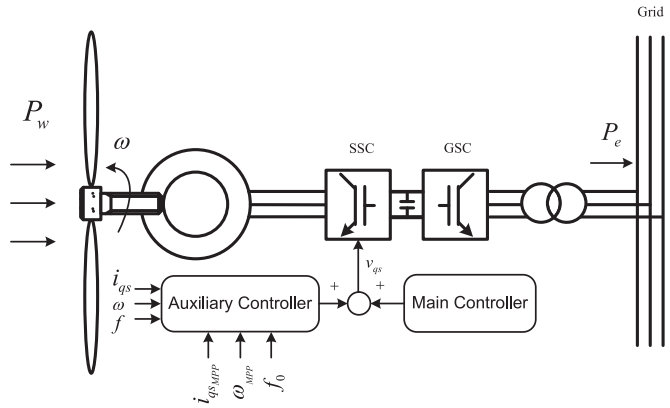

Fig. 3. General structure of FPC-based wind turbine equipped with the proposed controller.

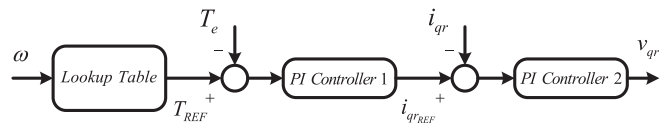

Fig. 4. Main speed (MPP) control scheme [5, p. 838].

as the Lyapunov function leads to the following laws for updating the parameters:

$$\begin{cases} r_1 = -x_1\xi_1 + \alpha_3 x_1 \xi_2 \\ r_2 = -x_2\xi_1 + \alpha_3 x_2 \xi_2 \end{cases} \tag{26}$$

This adaptive controller guarantees stable frequency support behavior of the auxiliary controller in the presence of unknown WECS parameters. General structure of the DFIG-based and FPC-based wind turbines equipped with the proposed controller are depicted in Figs. 2 and 3, respectively. The main controller is shown in Fig. 4 where the parameters of PI controllers are given in [5, p. 838]. Moreover, the lookup table block is the well-known quadratic equation, i.e., $T_{\mathrm{REF}} = k\omega^2$, where k is a constant number. In this study, the constant k is equal to 0.56 [27].

C. Analysis and Evaluation of Disturbances

This subsection is devoted to analysis and evaluation of two mentioned disturbances, i.e., w_1 and w_2. Due to similarity of analysis, only the influence of uncertain wind power input is discussed here.

With the proposed controller, the observable part of overall dynamical system equations reduces to:

$$\dot{\boldsymbol{\xi}} = \underbrace{\begin{pmatrix} 0 & 1 \\ -k_1 & -k_2 \end{pmatrix}}_{A} \boldsymbol{\xi} + \begin{pmatrix} 0 \\ (\gamma_2 + \gamma_3 x_1)\, h(t) \end{pmatrix} \tag{27}$$

where $\boldsymbol{\xi} = \left(\begin{smallmatrix} \xi_1 \\ \xi_2 \end{smallmatrix}\right)$ and $h(t) = \beta_1 w_1$. As it was stated before, k_1 and k_2 are chosen such that matrix A is asymptotically stable. Thus, there exists positive definite matrices $P = \left(\begin{smallmatrix} p_1 & p_3 \\ p_2 & p_4 \end{smallmatrix}\right) > 0$ and $Q > 0$ that satisfy the Lyapunov equation [26, p. 211]:

$$Q = -\left(A^T P + PA\right) = Q^T \tag{28}$$

The following Lyapunov function for the dynamical system (27):

$$V = \frac{1}{2}\boldsymbol{\xi}^T P \boldsymbol{\xi} \tag{29}$$

results in

$$\dot{V} = -\boldsymbol{\xi}^T Q \boldsymbol{\xi} + (\xi_1 p_3 + \xi_2 p_4)\,(\gamma_2 + \gamma_3 x_1)\, h(t) \tag{30}$$

Moreover, as the control is limited ($|u| < U^{\max}$), using the simple Lyapunov function $V(x_1) = \frac{1}{2}x_1^2$ for the first dynamical equation of (9) reveals that the state variable x_1 is confined in the limited range:

$$|x_1| < \frac{\beta U^{\max}}{\alpha_1} = X_1^{\max} \tag{31}$$

From both (30) and (31), and also the well-known inequality $\lambda_{\min}(Q)|\boldsymbol{\xi}|^2 \le \boldsymbol{\xi}^T Q \boldsymbol{\xi}$ [25], it can be concluded that:

$$\dot{V} \le -\lambda_{\min}(Q)|\boldsymbol{\xi}|^2 + k_{\max}|\boldsymbol{\xi}| \tag{32}$$

where

$$k_{\max} = \left(\max\{|p_3|, |p_4|\}\right)\left(|\gamma_2|_{\max} + |\gamma_3||X_1^{\max}|\right) h_{\max}$$

and $\lambda_{\min}(Q)$ is the minimum eigenvalue of the matrix Q. Moreover, $h_{\max} = \max\{h(t)\} = \max\{\beta_1 w_1\}$. The stability is guaranteed for

$$r^* = \frac{k_{\max}}{\lambda_{\min}(Q)} \le |\boldsymbol{\xi}| \tag{33}$$

Thus, the observable states remain limited within a ball with radius r^* in the presence of uncertain wind input. As $\lambda_{\min}(Q)$ becomes greater, $\boldsymbol{\xi}$ gets closer to the origin.

Uncertain wind input also affects the zero dynamics part. Based on (12), the zero dynamics part changes to:

$$\dot{\eta} = \frac{\alpha_2 \gamma_2 \eta}{\gamma_1 + \gamma_3 \eta} + h(t) = \frac{n\eta}{\eta + m} + h(t) \tag{34}$$

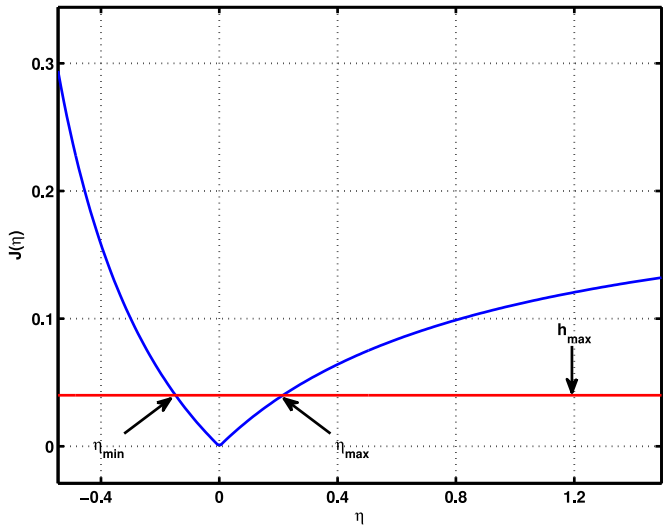

Fig. 5. Zero dynamics boundedness condition in the presence of uncertain wind input.

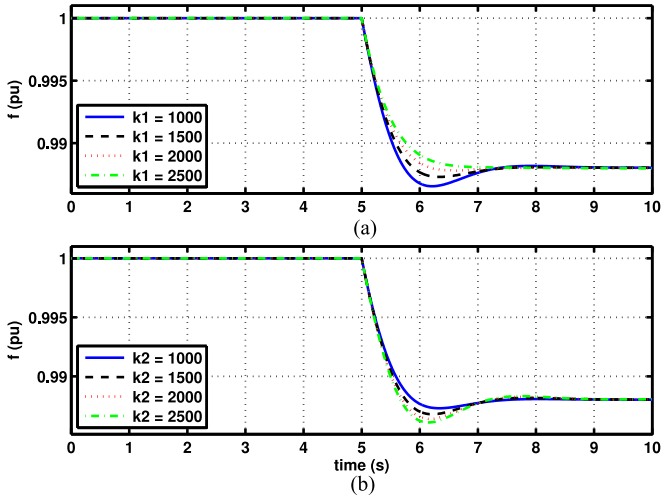

Fig. 6. Impact of different values of controller parameters (a) k_1 ($k_2 = 1000$), and (b) k_2 ($k_1 = 1500$) on WECS frequency behavior.

where

$$n = \frac{\alpha_2 \gamma_2}{\gamma_3}, \quad m = \frac{\gamma_1}{\gamma_3}$$

Using

$$V(\eta) = \frac{1}{2} \frac{\eta^2}{(\eta + m)^2} \tag{35}$$

as the Lyapunov function results in

$$\dot{V}(\eta) = \frac{mn\eta^2}{(\eta + m)^4} + \frac{m\eta}{(\eta + m)^3} \times h(t)$$

If $\dot{V}(\eta) < 0$, the state variable η remains bounded. In a conservative manner, to guarantee $\dot{V}(\eta) < 0$, it is sufficient that:

$$h_{\max} < J(\eta) = \frac{-n|\eta|}{\eta + m} \tag{36}$$

Equation (36) is illustrated in Fig. 5. For $\eta < \eta_{\min}$ or $\eta > \eta_{\max}$ derivative of the Lyapunov function is negative and thus, η is asymptotically confined in interval $[\eta_{\min}, \eta_{\max}]$.

It should be noted that a similar analysis can be carried out to ensure that the states remain bounded for load or generation changes in network.

IV. Controller Performance Evaluation

To evaluate the performance of the designed controller, the proposed controller is embedded into VSWT detailed model. This detailed model includes main (MPP) as well as the proposed controller, while pitch control is not considered since the VSWT is assumed to be variable-speed fixed-pitch (VSFP). There are numerous representations which model the electrical part of VSWT. Different state variables selections result in different representations. The current and flux models are the two well-known models of electrical part of VSWTs [27]. The current model is preferred whenever the PVdq control or vector control is applied in the induction based wind turbine structure.

The state and input vectors corresponding to this model are as follow:

$$\mathbf{x}_{\text{Detailed Model}} = [i_{\text{ds}}, i_{\text{qs}}, i_{\text{qs}}, i_{\text{qr}}] \tag{37}$$

$$\mathbf{u}_{\text{Detailed Model}} = [v_{\text{ds}}, v_{\text{qs}}, v_{\text{qs}}, v_{\text{qr}}] \tag{38}$$

where v and i represent the per unit value of voltage and current, respectively. These state variables in conjunction with the mechanical rotational speed ω complete the detailed model of VSWT. This detailed representation is stated in [27] and its electrical part is as follows:

$$\dot{\mathbf{x}}_{\text{Detailed Model}} = \overline{A}\mathbf{x}_{\text{Detailed Model}} + \overline{B}\mathbf{u}_{\text{Detailed Model}} \tag{39}$$

where $\overline{A}$ and $\overline{B}$ are the system and control matrices, respectively. As stated before, the pitch control scheme is neglected in this study. Moreover, the drive train is represented using the single mass model. This rotor mechanical equation completes the detailed representation as follows:

$$\frac{d}{dt}\omega = \frac{1}{2H}(T_m - T_e) \tag{40}$$

where T_m and T_e are mechanical and electromagnetic torques, respectively and ω is the rotational speed. The electromagnetic torque in terms of state variables is:

$$T_e = X_m (i_{\text{dr}} i_{\text{qs}} - i_{\text{qr}} i_{\text{ds}}) \tag{41}$$

The performance of proposed controller is investigated in the following subsections considering different scenarios.

A. Effect of Different Controller Parameters

The WECS inertial frequency response is affected by the controller parameters k_1 and k_2. These parameters determine the transient behavior characteristics such as settling time and damping ratio. As it was stated before, these controller parameters must be positive to ensure the stability of overall system. Their effects are depicted in Figs. 6.(a) and 6.(b), respectively. Wind power penetration level is assumed to be 30% and a step load change $\Delta P_L = 0.2$ pu is applied to the power system at

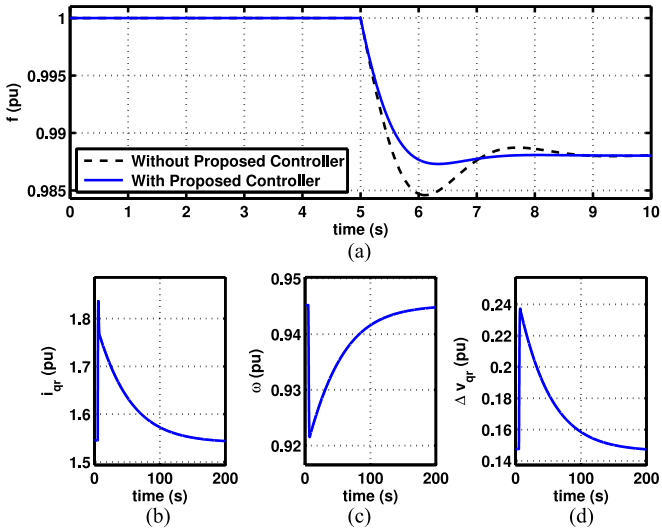

Fig. 7. (a) Frequency response result from joint operation of conventional units equipped with droop characteristic and VSWT equipped with or without the proposed controller, (b) corresponding quadrature current component, (c) corresponding rotational speed, and (d) required control signal due to 0.2 pu load increment at $t = 5$ s ($k_1 = 1500$ and $k_2 = 1000$).

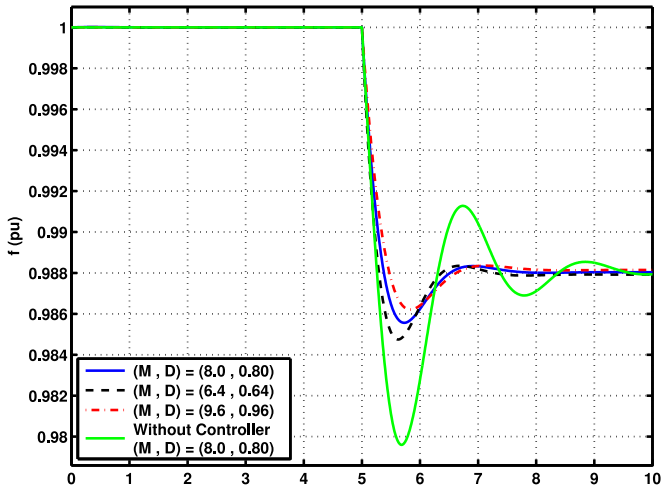

Fig. 8. Impact of uncertainty in power system characteristics on system frequency behavior with VSWT equipped with the proposed controller ($\Delta P_L = 0.2$ pu, $k_1 = 1500$, and $k_2 = 1000$).

$t = 5$ s. As it can be seen, to achieve the optimal frequency response, the controller parameters must be chosen with careful attention. High k_1 and low k_2 values are preferable. However, some operational limitations such as maximum allowable variations in WECS output power as well as desirable behavior in the recovery period affect controller parameters selection. A suitable set of controller parameters guarantees not only fast controller reaction, but also negligible transient recovery period.

B. Effect of Droop Response of Conventional Units

As stated before, the turbine-governors have been assumed to be slower than the designed VSWT controller, and hence not considered in the design process. However, their dynamics can be analyzed in the simulations that follow. To evaluate the droop response of the conventional units, the following transfer functions are utilized for the sake of simulation [22]:

$$T_{\mathrm{Gov}} = \frac{1}{0.08s + 1}$$

$$T_{\mathrm{Tur}} = \frac{1}{0.40s + 1}$$

The equivalent droop of power system is assumed to be $R = 1/16$. The effect of joint operation of droop response of conventional units and VSWTs equipped with or without the proposed controller is illustrated in Fig. 7.(a). The controller parameters are set to be $k_1 = 1500$ and $k_2 = 1000$, and it is assumed that the power system is subjected to the step load change $\Delta P_L = 0.2$ pu. Similar penetration level is considered here. From Fig. 7.(a), it could be concluded that application of the mentioned controller in the VSWT structure results in effective enhancement in the system frequency response. As shown, no oscillatory behavior is seen. The frequency nadir has improved from 0.984 pu to 0.987 pu ($0.003 \times 60 = 0.18$ Hz). Moreover, the initial rate of change of frequency is also enhanced. The corresponding rotor quadrature current and rotational speed are illustrated in Figs. 7.(b) and 7.(c), respectively. As these figures show, with the proposed controller, VSWT releases its stored kinetic energy immediately after the disturbance and then restores to MPP rather slow. This results in negligible recovery period. The required control signal is depicted in Fig. 7.(d).

C. Uncertainty in Power System Characteristics

It was shown in Section III that the performance of the proposed controller depends on the power system characteristics. Some methods have been proposed to estimate the values of power system parameters M and D [28]. However, lack of exact data is a general problem in power system dynamics studies. Moreover, these parameters vary over the time. Thus, the effect of parameter uncertainties on the proposed controller performance must be analyzed. Fig. 8 illustrates the impacts of $\pm 20\%$ variations in M and D parameters on the system frequency response. It is assumed that the original values of parameters M and D are 8 s and 0.8 pu, respectively. As this figure shows, even with high uncertainty in the system parameters, the overall frequency behavior is improved in comparison with the case in which no additional power is provided by VSWT.

D. Investigation of VSWT Recovery Period

Transient recovery time is the time interval in which the VSWT output power is temporarily reduced below its primary operating point and causes VSWT to restore to MPP. Appropriate co-ordination between the droop setting of conventional units and the parameters of proposed control accelerates the frequency regulation task and causes VSWT to return to the MPP as fast as possible. In other words, this co-ordination results in decreasing the recovery period of VSWTs participating in the power frequency control task. The concept of the co-ordination is depicted in Fig. 9, where various droop characteristics are studied. Co-ordination can be handled easily by means of a lookup table, in which associated with system equivalent droop

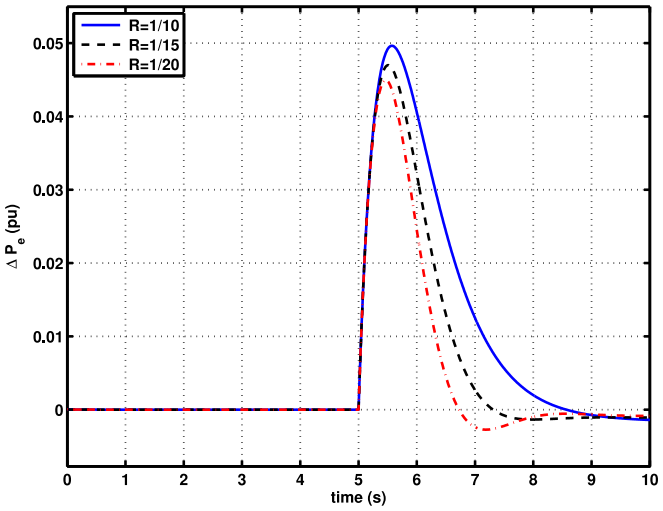

Fig. 9. Effect of different droop characteristics on provided frequency support by VSWT ($\Delta P_L = 0.2$ pu, $k_1 = 1500$, and $k_2 = 1000$).

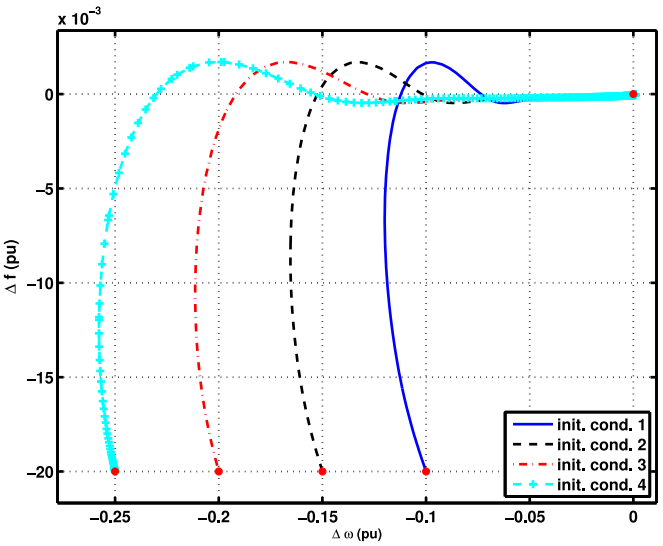

Fig. 10. x_2-x_3 trajectories corresponding to different initial conditions ($k_1 = 1500$ and $k_2 = 1000$).

the appropriate controller parameters are reported. The importance of co-ordination is obvious and as can be seen, suitable choice of controller parameters results in negligible transient recovery period time.

E. Enhancement in Critical Conditions

As it was proved in Section III, the proposed controller guarantees that for each initial condition, the state variables remain stable. Moreover, the frequency response is also improved. It should be noted that the predicted enhancement in the frequency behavior due to application of the proposed controller is amplified when the power system encounters significant load-generation mismatches. In other words, in critical conditions, the provided power by the proposed controller increases as it is expected. Fig. 10 shows the trajectory of state variables x_2 and x_3 corresponding to severe initial conditions given in Table III.

TABLE III
INITIAL CONDITION USED IN SIMULATIONS

initial condition	x_1^0	x_2^0	x_3^0
init. cond. 1	0	−0.10	−0.02
init. cond. 2	0	−0.15	−0.02
init. cond. 3	0	−0.20	−0.02
init. cond. 4	0	−0.25	−0.02

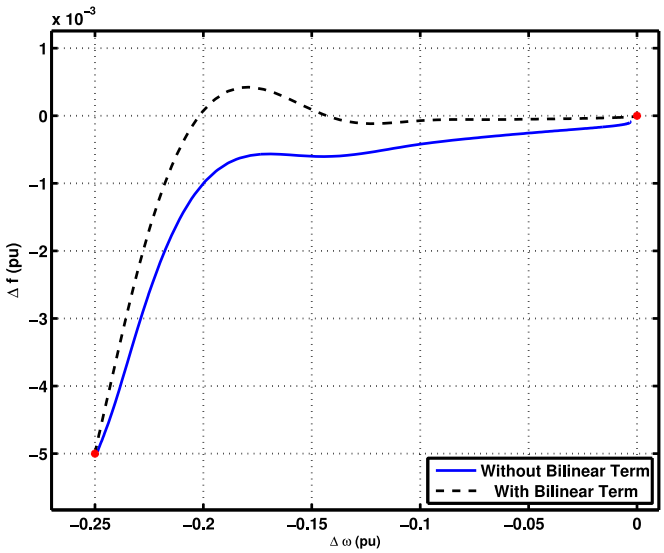

Fig. 11. x_2-x_3 trajectory corresponding to initial condition (0,−0.25,−0.005) with and without considering the bilinear term ($k_1 = 1500$ and $k_2 = 1000$).

It is clear that the predicted enhancement can be recognizable even under severe conditions.

Moreover, Fig. 11 illustrates the effect of bilinear term in (4) on the trajectories of states x_2-x_3 corresponding to the initial condition (0,−0.25,−0.005). As can be observed, considering the bilinear term results in an enhanced frequency regulation compared to the case of linearized WESC and power system model. This is the reason why the nonlinear controller lends itself to inertial frequency response of VSWTs.

F. Comparison with Conventional Controller

Traditionally, VSWT frequency support is provided by changing the reference point of main speed regulator which uses the PI controller. Thus, an optimal frequency response could not be expected with this conventional controller. However, the proposed controller uses the measurable state variables rather than the output signals to produce the appropriate control signal for an enhanced response. The states needed as the input of the proposed controller can be seen in Figs. 2 and 3 for DFIG-based and FPC-based wind turbines, respectively.

Fig. 12.(a) shows the superiority of the proposed controller in comparison with the conventional frequency controller. A 0.2 pu step load increment is considered as disturbance and the parameters of PI controller are equal to $K_I = 0.5$, $K_P = 0.5$ [21]. The frequency nadir values without frequency controller, with conventional controller, and with proposed controller are

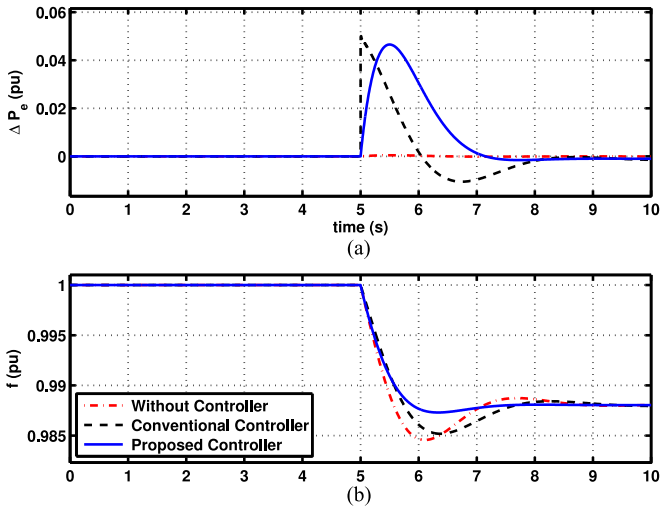

Fig. 12. Comparison between the response of proposed controller and conventional frequency controller (a) frequency response, (b) corresponding output power variation ($k_1 = 1500$, $k_2 = 1000$, $K_I = 0.5$, $K_P = 0.5$).

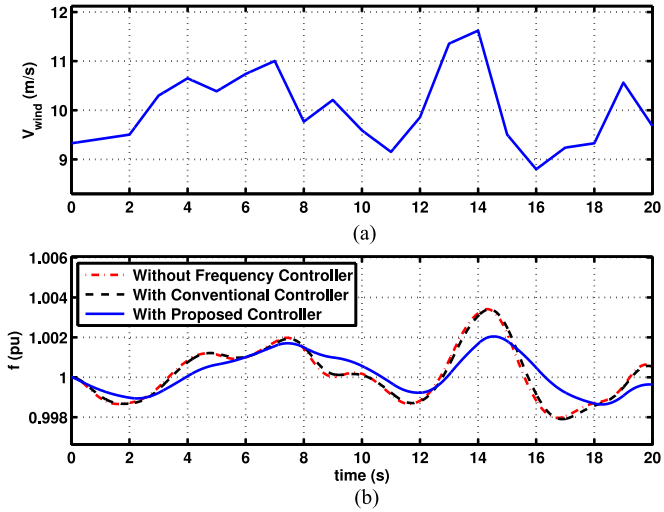

Fig. 13. (a) Wind speed profile, and (b) corresponding impacts on system frequency considering different scenarios for participation of VSWT in frequency regulation task.

0.984 pu, 0.985 pu, and 0.987 pu, respectively. Similar enhanced responses are seen with other disturbances. It should be noted that in contrast to the conventional frequency controller which changes the torque set point first, the provided supplementary signal in the proposed controller is directly injected into the rotor voltage. This not only results in enhanced aggregated frequency response, but also reduces the mechanical load on the WECS structure just after disturbances. Moreover, negligible transient recovery period could be expected with the proposed method.

The corresponding output power variations is depicted in Fig. 12.(b). With the proposed controller, VSWT rather quickly injects the additional power by decreasing its rotational speed and then restores MPP more smoothly than the conventional frequency controller. As it was expressed before, this results in negligible recovery period in comparison with the conventional frequency controller which shows an oscillatory behavior. In other words, there is a slight underproduction by VSWT during the recovery period in order to cancel out the initial overproduction.

G. Effect of Uncertain Wind Power Input

Up to now, it has been assumed that the wind input power is constant. However, the expected wind power variations due to wind speed volatility affect the power system. A realistic wind speed profile [29] is utilized for simulations. The wind speed profile and its corresponding impacts on power system frequency are depicted in Figs. 13.(a) and 13.(b), respectively. Three different cases are considered for the participation of VSWT in the frequency regulation task.

It was discussed in subsection III-C that the main functionality of the controller is preserved in presence of uncertain wind input. Thus, it can be claimed that the designed controller can be used regardless of wind speed variations. Moreover, as it is shown in Fig. 13, the impacts of intermittent wind speed on the system frequency are alleviated by using the proposed controller.

H. Effects of Limited Control and Nonlinear Operational Constraints

The effects of saturation in the control u were not considered in the previous subsections and it was assumed that the control variable u could change in the unlimited range. However, due to physical limitations such as maximum converter power and maximum allowable rotor speed variation, this assumption is not realistic. In fact, the control variable could change in a confined range, i.e., $|u| < U^{\max}$. Moreover, limitations in the VSWT output power variations ($|\Delta P_e| < P^{\max}$) as well as its rate of variation ($|dP_e/dt| < (dP/dt)^{\max}$) affect the provided frequency support by VSWT and these important nonlinear operational constraints must be considered in the controller performance evaluation as shown in Fig. 1.

A 0.2 pu load increment is considered as disturbance. The effects of the nonlinear constraints (limited control and operational constraints) on the wind turbine output power variations and power system frequency behavior are shown in Figs. 14.(a) and 14.(b), respectively. As it is expected and obvious from Fig. 14, these nonlinear constraints worsen normal frequency support of the proposed controller and postpone the regulation task. However, the main functionality of the controller is preserved even with nonlinear operational constraints.

To better show the superiority of the proposed controller, a comparison between its response and the response of a conventional PI controller, considering all mentioned nonlinear constraints, is also made. Figs. 15.(a) and 15.(b) comprise the wind turbine output power variations and the frequency response due to the application of the proposed controller and conventional controller, respectively. As shown, both controllers show similar response just after disturbance. This is mostly due to the nonlinear constraints which do not allow sudden changes in the output power of VSWTs. However, the superiority of proposed controller is demonstrated a few moments later due to the higher provided power during the frequency support period. Thus, the frequency nadir improves using the proposed controller.

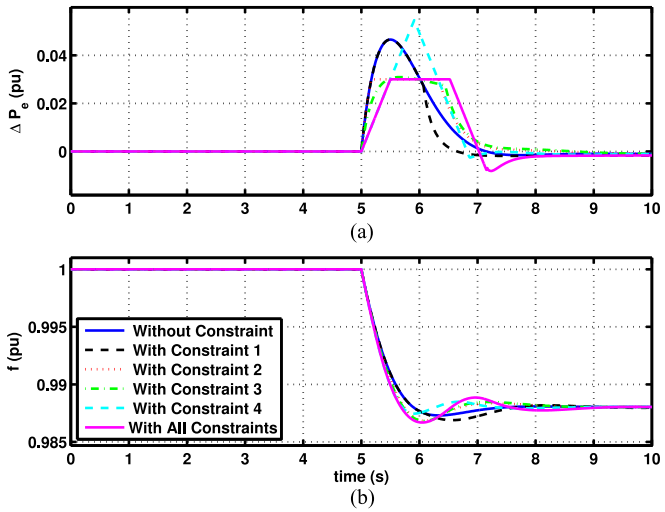

Fig. 14. Effect of nonlinear constraints (limited control and operational constraints) on (a) wind turbine output power variations, and (b) power system frequency behavior (Constraint 1: $U^{\max} = 0.1$, Constraint 2: $P^{\max} = 0.1$, Constraint 3: $(dU/dt)^{\max} = 0.07$, Constraint 4: $(dP/dt)^{\max} = 0.2$, $k_1 = 1500$, $k_2 = 1000$).

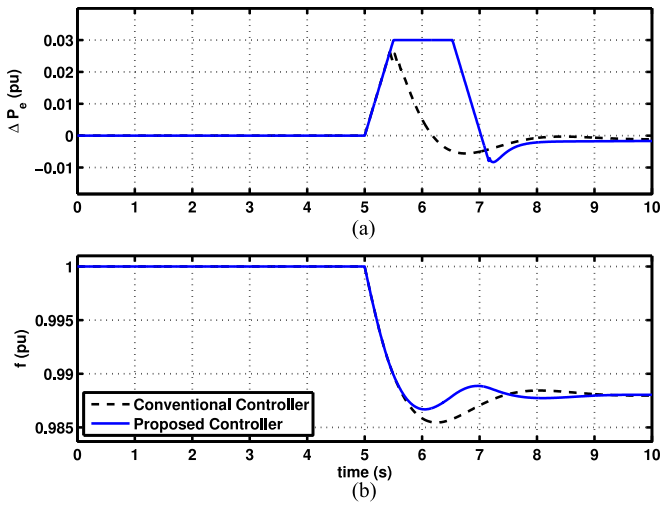

Fig. 15. Comparison between the response of proposed controller and conventional frequency controller considering nonlinear constraints (a) wind turbine output power variations, and (b) frequency response (Constraint 1: $U^{\max} = 0.1$, Constraint 2: $P^{\max} = 0.1$, Constraint 3: $(dU/dt)^{\max} = 0.07$, Constraint 4: $(dP/dt)^{\max} = 0.2$, $K_I = 0.5$, $K_P = 0.5$, $k_1 = 1500$, $k_2 = 1000$).

V. Conclusion

This paper proposes a new nonlinear auxiliary controller using the input-output feedback linearization method to enable VSWTs inertial frequency response. The proposed nonlinear controller is designed based on the nonlinear system model without neglecting higher order terms of wind turbine output power. The regulated rotor voltage of VSWT successfully emulates inertial response of synchronous generators by changing the output power of VSWT in response to frequency deviations. To eliminate the impacts of unknown parameters in WECS structure, an adaptive controller is also suggested. The validity of the designed controller is confirmed by its application to the VSWT detailed model, which ensures that it can be embedded in the VSWT structure. Performance of the controller with diverse controller parameters is investigated. The proposed controller with appropriate parameters guarantees fast response even to large frequency deviations. Joint operation of conventional units with the droop characteristic and VSWT with the proposed controller is also evaluated with sensitivity analysis on different power system parameters. It is proved that an effective enhancement in the frequency behavior can be achieved by integration of the proposed controller in VSWT structure. It is also emphasized that appropriate co-ordination between the conventional units and VSWTs equipped with the proposed controller results in negligible transient recovery period. Moreover, the frequency support behavior of the proposed controller is studied in presence of fluctuating wind power input. It is proved that with this disturbance, using the proposed controller results in a smoother frequency response. The effect of practical nonlinear operational constraints including the maximum rate of change of output power is also analyzed. It is shown that these nonlinearities postpone the frequency support of the proposed controller. Furthermore, the advantages of the proposed controller over the conventional PI controller are verified.

References

[1] International Energy Agency, Paris, France. (2012). [Online]. Available: http://www.iea.org/publications/scenariosandprojections/

[2] "20% wind energy by 2030: Increasing wind energy's contribution to U.S. electricity supply," U.S. Dept. Energy, Oak Ridge, TN, USA, Tech. Rep. DOE/GO-102008-2567, Jul. 2008. [Online]. Available: http://energy.gov/sites/prod/files/2013/12/f5/41869.pdf

[3] "Estimates of windy land area and wind energy potential by state for areas." (2010). [Online]. Available: http://www.windpoweringamerica.gov/docs/wind_potential_80m_30percent.xlsx

[4] "Global wind report annual market update 2014." (2014). [Online]. Available: http://www.gwec.net/wp-content/uploads/2015/03/GWEC_Global_Wind_2014_Report_LR.pdf

[5] T. Ackermann, *Wind Power in Power Systems*, 2nd ed. Hoboken, NJ, USA: Wiley, 2012.

[6] F. D. Bianchi, H. De Battista, and R. J. Mantz, *Wind Turbine Control Systems: Principles, Modelling and Gain Scheduling Design*. Berlin, Germany: Springer-Verlag, 2007.

[7] S. Kuenzel, L. P. Kunjumuhammed, B. C. Pal, and I. Erlich, "Impact of wakes on wind farm inertial response," *IEEE Trans. Sustain. Energy*, vol. 5, no. 1, pp. 237–245, Jan. 2014.

[8] Y. Liu, J. R. Gracia, T. J. King, and Y. Liu, "Frequency regulation and oscillation damping contributions of variable-speed wind generators in the U.S. eastern interconnection (EI)," *IEEE Trans. Sustain. Energy*, vol. 6, no. 3, pp. 951–958, Jul. 2015.

[9] P. K. Keung, P. Li, H. Banakar, and B. Ooi, "Kinetic energy of wind-turbine generators for system frequency support," *IEEE Trans. Power Syst.*, vol. 24, no. 1, pp. 279–287, Feb. 2009.

[10] N. R. Ullah, T. Thiringer, and D. Karlsson, "Temporary primary frequency control support by variable speed wind turbines–potential and applications," *IEEE Trans. Power Syst.*, vol. 23, no. 2, pp. 601–612, May 2008.

[11] M. Akbari and S. M. Madani, "Analytical evaluation of control strategies for participation of doubly fed induction generator-based wind farms in power system short-term frequency regulation," *IET Renew. Power Gener.*, vol. 8, no. 3, pp. 324–333, Apr. 2014.

[12] J. Lee, E. Muljadi, P. Sorensen, and Y. C. Kang, "Releasable kinetic energy-based inertial control of a DFIG wind power plant," *IEEE Trans. Sustain. Energy*, vol. 7, no. 1, pp. 279–288, Jan. 2016.

[13] GE Energy, Atlanta, GA, USA, "WindINERTIA fact sheet—GE Energy." (2009). [Online]. Available: http://site.ge-energy.com/prod_serv/products/renewable_energy/en/downloads/GEA17210.pdf

[14] Enercon, Bremen, Germany, "Integrated solutions for compliance with demanding international grid codes." (Nov. 30, 2016). [Online]. Available: http://www.enercon.de/en/technology/grid-technology/, Accessed on: Nov. 30, 2016.
[15] N. Nguyen and J. Mitra, "An analysis of the effects and dependency of wind power penetration on system frequency regulation," *IEEE Trans. Sustain. Energy*, vol. 7, no. 1, pp. 354–363, Jan. 2016.
[16] V. Gevorgian, Y. Zhang, and E. Ela, "Investigating the impacts of wind generation participation in interconnection frequency response," *IEEE Trans. Sustain. Energy*, vol. 6, no. 3, pp. 1004–1012, Jul. 2015.
[17] F. Teng and G. Strbac, "Assessment of the role and value of frequency response support from wind plants," *IEEE Trans. Sustain. Energy*, vol. 7, no. 2, pp. 586–595, Apr. 2016.
[18] F. Baccino, F. Conte, S. Grillo, S. Massucco, and F. Silvestro, "An optimal model-based control technique to improve wind farm participation to frequency regulation," *IEEE Trans. Sustain. Energy*, vol. 6, no. 3, pp. 993–1003, Jul. 2015.
[19] M. Hwang, E. Muljadi, J. W. Park, P. Sorensen, and Y. C. Kang, "Dynamic droop-based inertial control of a doubly-fed induction generator," *IEEE Trans. Sustain. Energy*, vol. 7, no. 3, pp. 924–933, Jul. 2016.
[20] N. G. Hingorani and L. Gyugyi, *Understanding FACTS: Concepts and Technology of Flexible AC Transmission Systems*. Hoboken, NJ, USA: Wiley, 2000.
[21] J. B. Ekanayake, N. Jenkins, and G. Strbac, "Frequency response from wind turbines," *Wind Eng.*, vol. 32, no. 6, pp. 573–586, Dec. 2008.
[22] H. Bevrani, *Robust Power System Frequency Control*. Berlin, Germany: Springer, 2014.
[23] T. H. Mohamed, J. Morel, H. Bevrani, and A. A. Hassan, "Model predictive based load frequency control design concerning wind turbines," *Int. J. Elect. Power Energy Syst.*, vol. 43, no. 1, pp. 859–867, Dec. 2012.
[24] A. J. Wood and B. F. Wollenberg, *Power Generation, Operation, and Control*. Hoboken, NJ, USA: Wiley, 2012.
[25] H. K. Khalil, *Nonlinear Systems*, 3rd ed. Englewood Cliffs, NJ, USA: Prentice Hall, 2002.
[26] K. J. Astrom and B. Wittenmark, *Adaptive Control*, 2nd ed. Englewood Cliffs, NJ, USA: Prentice-Hall, 1995.
[27] C. E. Ugalde-Loo, J. B. Ekanayake, and N. Jenkins, "State-space modeling of wind turbine generators for power system studies," *IEEE Trans. Ind. Appl.*, vol. 49, no. 1, pp. 223–232, Jan. 2013.
[28] M. Shamirzaee, H. Ayoubzadeh, D. Farokhzad, F. Aminifar, and H. Haeri, "An improved method for estimation of inertia constant of power system based on polynomial approximation," in *Proc. Smart Grid Conf.*, Dec. 2014, pp. 1–7.
[29] "Database of wind characteristics located at DTU, Denmark." (2013). [Online]. Available: http://www.winddata.com

Mohammadreza Toulabi received the B.Sc. and M.Sc. degrees in electrical engineering from Sharif University of Technology, Tehran, Iran, in 2010 and 2012, respectively. He is currently working toward the Ph.D. degree in electrical engineering at Sharif University of Technology.

Ahmad Salehi Dobakhshari received the B.Sc., M.Sc., and Ph.D. degrees from Sharif University of Technology, Tehran, Iran, in 2006, 2008, and 2014, respectively, all in electrical engineering. He was with Monenco Iran Consulting Engineers Company, Tehran, from 2009 to 2013, and with Mapna Group, Tehran, from 2014 to 2015. In 2016, he joined the Faculty of Engineering, University of Guilan, Rasht, Iran. His current research interests include utilizing wide-area measurements in power systems, fault location, renewable energy, and smart grid.

Ali Mohammad Ranjbar received the M.Sc. degree in electrical engineering from the University of Tehran, Tehran, Iran, in 1967 and the Ph.D. degree in electrical engineering from Imperial College of London, London, U.K., in 1975.

He is currently a Professor in the School of Electrical Engineering, Sharif University of Technology, Tehran. His research interests include power system control and protection.